Dynamics of nonlinear excitations of helically confined charges

A. V. Zampetaki,[1] J. Stockhofe,[1] and P. Schmelcher[1,2]
[1]*Zentrum für Optische Quantentechnologien, Universität Hamburg, Luruper Chaussee 149, 22761 Hamburg, Germany*
[2]*The Hamburg Centre for Ultrafast Imaging, Luruper Chaussee 149, 22761 Hamburg, Germany*
(Received 22 July 2015; published 2 October 2015)

We explore the long-time dynamics of a system of identical charged particles trapped on a closed helix. This system has recently been found to exhibit an unconventional deformation of the linear spectrum when tuning the helix radius. Here we show that the same geometrical parameter can affect significantly also the dynamical behavior of an initially broad excitation for long times. In particular, for small values of the radius, the excitation disperses into the whole crystal whereas within a specific narrow regime of larger radii the excitation self-focuses, assuming finally a localized form. Beyond this regime, the excitation defocuses and the dispersion gradually increases again. We analyze this geometrically controlled nonlinear behavior using an effective discrete nonlinear Schrödinger model, which allows us among others to identify a number of breatherlike excitations.

DOI: 10.1103/PhysRevE.92.042905 PACS number(s): 05.45.−a, 37.10.Ty, 37.90.+j, 45.90.+t

I. INTRODUCTION

Whereas the harmonic approximation of interactions provides valuable information about the stability and the propagation of small amplitude excitations in crystals formed by interacting particles, their real-time dynamics as well as their thermal and transport properties are typically subject to some degree of nonlinearity [1]. Among the most prominent manifestations of such a nonlinearity are the self-focusing or self-trapping [2–4] of initial wave packet excitations and the existence of nonspreading excitations such as breathers and kinks [5–7]. For discrete systems, a prototype equation incorporating these features is the so-called discrete nonlinear Schrödinger (DNLS) equation consisting of a linear (dispersive) coupling and a cubic nonlinear term [8], used to model plenty of systems ranging from coupled optical waveguides [9–11] and Bose-Einstein condensates [12–14] to transport in DNA molecules [15–17]. The standard spatial arrangement of sites in most of such one-dimensional (1D) studies is that of a straight equidistant chain in which the coupling (hopping) is restricted to nearest neighbors.

Nontrivial lattice geometries for 1D discrete nonlinear systems have also been studied and have been found to lead to intriguing new phenomena owing to the interplay between geometry and nonlinearity. In particular, in curved 1D lattices embedded in a 2D space the bending can act as a trap of excitations and induce a symmetry breaking of nontopological solitons [18]. For a 3D space, the helicoidal lattice structure, such as that of DNA molecules, is found to enhance the existence and stability of discrete breathers [19,20]. Furthermore, a curved geometry has been proven to induce nonlinearity in systems where the underlying interactions are harmonic [21,22].

In the present work we examine the interplay between nonlinearity and geometry in a system of identical charged particles, confined on a curved 1D manifold embedded in the 3D space, namely a closed (toroidal) helix. In a previous work [23], we have shown that in such a system, a tuning of the geometry controlled by the helix radius, leads to an unconventional deformation of the phononic band structure including a regime of strong degeneracy. As a consequence, the propagation of small amplitude localized excitations is affected significantly and a specific geometry exists at which the excitations remain localized up to long times. A natural question therefore arises as to what would be the long time dynamics of a general excitation and whether there is some geometrically controllable degree of nonlinearity inherent in the system, which can alter the propagation characteristics.

We provide an answer to this question by studying the time propagation of an initially broad excitation on the crystal of charges. We find that for values of the helix radius far from the degeneracy regime, the excitation initially spreads with multiple subsequent revivals due to the closed shape of the crystal. Within the degeneracy regime, however, the initial excitation focuses in the course of propagation reaching finally a rather localized state, serving as a hallmark of the existing nonlinearity. In order to quantify this nonlinearity we construct an effective DNLS model with additional nonlocal nonlinear terms [24,25]. Such a model is found to capture qualitatively well the localization and dispersion features of the original dynamics, providing a deeper insight into the observed effect. Even more, it gives us the opportunity to identify some discrete breatherlike excitations at the degenerate geometry, thus adding to the dynamical picture.

The structure of this work is as follows. In Sec. II we describe our system, commenting also on its linearized behavior. In Sec. III we present our results for the time evolution of an excitation in the crystal for different geometries. In Sec. IV we construct an effective DNLS model for our system at the geometries of interest and in Sec. V we use it to identify some breatherlike excitations. Finally, Sec. VI contains our conclusions.

II. SETUP AND LINEARIZATION

We consider a system of N identical charges of mass m_0, which interact via repulsive Coulomb interactions and are confined to move on a 1D toroidal helix, parametrized as

$$\mathbf{r}(u) = \begin{pmatrix} (R + r\cos(u))\cos(au) \\ (R + r\cos(u))\sin(au) \\ r\sin(u) \end{pmatrix}, \quad u \in [0, 2M\pi]. \qquad (1)$$

In Eq. (1) R denotes the major radius of the torus [Fig. 1(a)], h is the helix pitch, and r the radius of the helix (minor

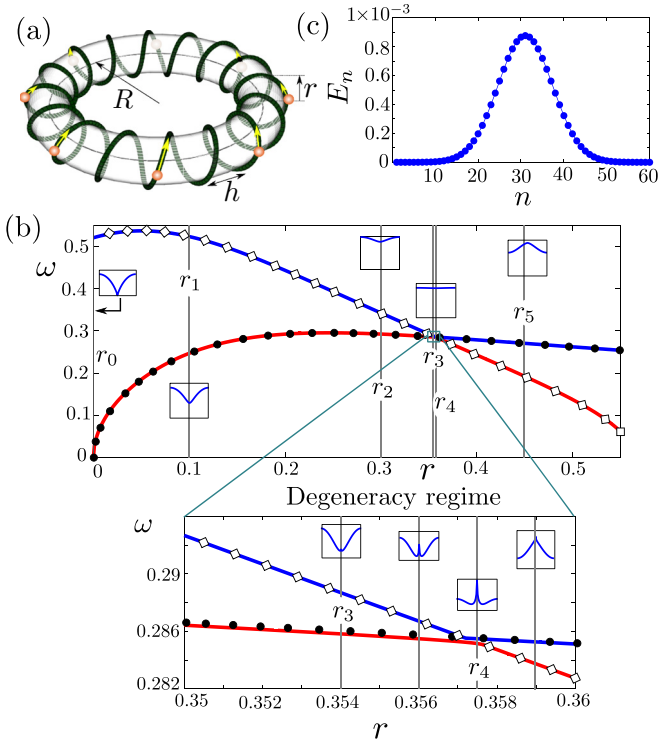

FIG. 1. (Color online) (a) Equidistant configuration of ions confined on the toroidal helix for $\nu = \frac{1}{2}$ and $N = 8$. The yellow arrows indicate the initial velocities of the particles. (b) Highest (solid blue line) and lowest (solid red line) frequencies of the linearization spectrum around the equilibrium equidistant configuration as a function of r for $N = 60$ particles. The black dots and the empty diamonds refer to the frequencies corresponding to the center of mass and the out of phase mode respectively. The vertical lines mark the radii of the helix we use in our calculations. The small insets depict the form of the respective vibrational band structures $\omega(k)$ at the corresponding values of r. (c) Initial local energy E_n profile as a function of the particle index n.

radius of the torus), whereas $a = \frac{1}{M}$ stands for the inverse number of windings $M = \frac{2\pi R}{h}$. The total effective interaction potential, which results from the constrained motion of the charges on the helical manifold, reads $V(u_1,u_2,\dots u_N) = \frac{1}{2}\sum_{i,j=1,i\neq j}^{N} \frac{\lambda}{|\mathbf{r}(u_i)-\mathbf{r}(u_j)|}$, where u_j denotes the coordinate of particle j and λ is the coupling constant characterizing the standard Coulomb interactions.

Then the Lagrangian of the system in terms of the u_i coordinates is given by

$$L(\{u_i,\dot{u}_i\}) = \frac{1}{2}m_0\sum_{i=1}^{2}|\partial_{u_i}\mathbf{r}(u_i)|^2\dot{u}_i^2 - \frac{1}{2}\sum_{i,j=1,i\neq j}^{N}\frac{\lambda}{|\mathbf{r}(u_i)-\mathbf{r}(u_j)|}, \quad (2)$$

where $\mathbf{r}(u)$ refers to the parametrization of the toroidal helix given in Eq. (1). Note that the geometry of the constraint manifold enters the Lagrangian of Eq. (2) in both the interaction and the kinetic energy, due to the position-dependent factor $|\partial_{u_i}\mathbf{r}(u_i)|^2$. If desired, the latter factor can be removed by transforming to arc-length parametrization $s(u) = \int|\partial_u\mathbf{r}(u)|du$, resulting in the familiar second time derivative terms in the Euler-Lagrange equations of motion for the $s_i(t) = s[u_i(t)]$ [26], at the cost, however, of losing the explicit analytical form for the interaction energy.

We choose dimensionless units by scaling all our physical quantities (e.g., position x, time t, and energy E) with λ, m_0, and $2h/\pi$ as follows:

$$\tilde{x} = \frac{x\pi}{2h}, \quad \tilde{t} = t\sqrt{\frac{\lambda\pi^3}{8m_0h^3}}, \quad \tilde{E} = \frac{2Eh}{\lambda\pi}, \quad \tilde{m}_0 = 1, \quad \tilde{\lambda} = 1,$$

omitting in the following the tilde for simplicity.

At commensurate fillings, i.e., $M = nN$, $n = 1,2,\dots$ with the filling factor being $\nu = 1/n \leqslant 1$, it is found that for values of the helix radius r up to a critical point r_c the ground-state configuration of such a system is the equidistant polygonic configuration $u_j^{(0)} = 2(j-1)\pi n$ [Fig. 1(a)]. This configuration loses its stability at r_c undergoing a zigzag bifurcation [23].

We focus in this work on the dynamical behavior of charged particles confined on the toroidal helix in the region $r < r_c$, where the ground state is still the polygonic one. We have shown in Ref. [23] that in such a region the linear spectrum of the system changes dramatically with tuning the radius of the helix r, a fact that crucially affects the propagation of small amplitude localized excitations. Specifically, it was found that the width of the linear spectrum decreases as one approaches a point r_d of strong degeneracy from below and increases again beyond that point, while interchanging the character between the eigenmodes corresponding to the highest and the lowest frequencies [Fig. 1(b)]. In fact, since the degeneracy is not complete, it is better to refer to a degeneracy regime within which the inversion of the spectrum is gradually achieved while its width remains small [Fig. 1(b) (inset)]. We consider in this work six different geometries, each corresponding to a different value of r, covering all the regions with a qualitatively different linear spectrum [Fig. 1(b)] from the ring limit ($r_0 = 0$) to the degeneracy (r_3,r_4) and the inversion (r_5) regime. We focus on the case of half filling $\nu = \frac{1}{2}$ for $N = 60$ particles.

III. TIME PROPAGATION OF A GAUSSIAN EXCITATION

In this section we present and discuss the dynamical response of our system to an initial excitation. Although the physical results are in principle independent of the exact character of this excitation and the means used for its quantification, the determination of both is essential for the illustration and the theoretical description of our findings.

Dealing with classical systems and seeking an excitation measure whose total amount is conserved in time, the natural choice is a (to be defined) energy distribution associated with each particle, referred to hereafter as local energy E_n. Whereas the kinetic energy K consists of parts allocated to each individual particle, the potential energy cannot be uniquely partitioned, yielding different definitions of local energy [27–29]. Aiming for them to be strictly positive for all possible excitations (a considerably nontrivial requirement for systems with Coulomb interactions), we define our local energies E_n in a rather unconventional way, focusing on a

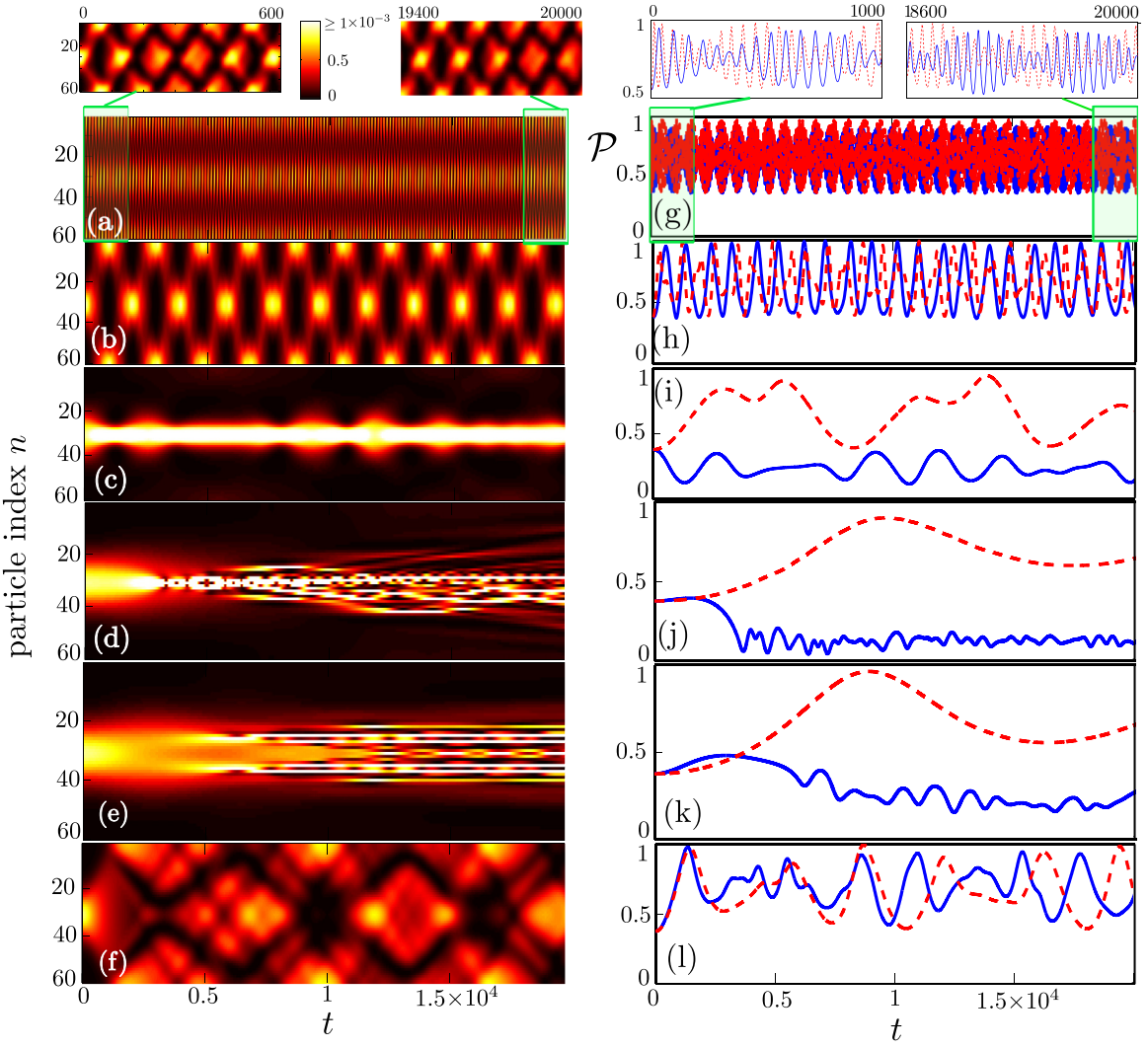

FIG. 2. (Color online) (a)–(f) Time evolution of the initial Gaussian excitation presented in Fig. 1(c) for $N = 60$, $\nu = 1/2$ for increasing r corresponding to the points (a) r_0, (b) r_1, (c) r_2, (d) r_3, (e) r_4, and (f) r_5 marked in Fig. 1(b). Colors encode the values of local energy E_n for each particle n and time t. For the same values of r panels (g)–(l) depict the time evolution of the normalized participation ratio $\mathcal{P}$ of the excitation. The solid blue lines are the results from our numerical simulations corresponding to (a)–(f), whereas the dashed red lines correspond to the results for a harmonic approximation of the potential.

positive decomposition of the harmonic interaction term [29]. Our complete definition and a more detailed discussion of local energies are provided in the Appendix.

We start with an initially broad excitation of a Gaussian profile in terms of local energies [Fig. 1(c)]. Since the local energies E_n depend trivially on the particles' velocities (contrary to what is the case for the particles' positions), the most straightforward way to obtain such a Gaussian local energy profile is by exciting the particles with a suitable velocity distribution. Of course, for a given local energy profile the magnitude of such a velocity distribution can be uniquely determined, but there is a freedom in the direction of the velocity for each particle. We choose here all the velocities to point in the positive direction [Fig. 1(a)].

The ensuing dynamics is shown in Figs. 2(a)–2(f). Obviously, the time evolution of the Gaussian excitation possesses a drastic dependence on the geometry, controlled by the helix radius r. In particular, for $r < r_d$ [Figs. 2(a), 2(b)] the excitation spreads into the whole crystal and refocuses almost periodically at the time instants when the left and the right propagating parts of the excitation meet and superimpose at the diametrically opposite point of the closed helix. As discussed in Ref. [23] the spreading velocity decreases as r is increased, following the width of the linear spectrum [Fig. 1(b)]. As the width becomes smaller the features of the time evolution alter significantly. Already at the point r_2 the excitation does not spread any more into the crystal, but it alternately focuses and again defocuses to its initial shape [Fig. 2(c)]. Even more surprisingly, within the degeneracy region [Figs. 2(d), 2(e)] the initial excitation undergoes a focusing after some time scale t_F [$t_F \approx 4000$ for Fig. 2(d), $t_F \approx 6000$ for Fig. 2(e)]. Subsequently, the wave packet loses its smooth envelope and fragments into a number of highly localized excitations. Depending on r, the routes towards such a localized state can be different, with the wave packet evolving initially one central peak [Fig. 2(d)] or two side peaks [Fig. 2(e)]. Another interesting feature within the degeneracy regime is that the reflection symmetry of the initial excitation profile can break

in the course of propagation, attaining after some time a significantly asymmetric form [Fig. 2(d)]. The direction of the asymmetry depends on the direction of the initial velocities of the particles. Beyond the degeneracy [Fig. 2(f)] the spreading of the excitation into the crystal reappears with a periodic refocusing but the propagation pattern is much different owing to the inverted form of the vibrational band structure.

In order to quantify the degree of focusing or localization of the excitation, we examine the time dependence of the normalized participation ratio

$$\mathcal{P} = \frac{1}{N} \frac{\left(\sum_{n=1}^{N} E_n\right)^2}{\sum_{n=1}^{N} E_n^2}. \tag{3}$$

Evidently, this quantity can take values between $1/N$ and 1, with $\mathcal{P} = 1$ signifying the case of a completely extended excitation where the energy is equipartitioned between all the particles and $\mathcal{P} = 1/N$ marking the opposite case of a fully localized excitation in a single particle. Note that the local energies E_n in (3) should be non-negative for the definition to make sense.

Our results, presented in Figs. 2(g)–2(l), support our discussion above. Especially the focusing of the excitation after t_F is evident in Figs. 2(j)–2(k). However, the subsequent drop in $\mathcal{P}$ is much stronger in Fig. 2(j) than in Fig. 2(k), in line with the observation that at $r = r_3$ the final localized state consists of less excited particles [Fig. 2(d)] than at $r = r_4$ [Fig. 2(e)].

In Ref. [23] it was demonstrated that a small localized initial excitation does not spread significantly for short times at the degeneracy point, in contrast to the behavior for other geometries. This fact was understood solely by an inspection of the linearization spectrum. Here, however, the situation is different. Not only the complete absence of spreading, but especially the existence of self-focusing calls for an account of the underlying nonlinearity. This is further emphasized and supported by Figs. 2(g)–2(l) where the results of the propagation within the harmonic approximation of the potential are also displayed. As long as the total amplitude of the initial excitation is small enough, the harmonic approximation works well. As the amplitude is increased this approximation will start to fail, and nonlinear effects are expected to show up. The results of the present work suggest that except for the amplitude, also the geometry allows to control the importance of the nonlinearity. Specifically, for the given amplitude and for geometries far from the degeneracy regime [Figs. 2(g), 2(h), 2(l)] the harmonic approximation qualitatively reproduces the exact time evolution of the participation ratio, although, as should be expected, there are quantitative deviations. In contrast, close to and within the degeneracy regime the harmonic approximation fails completely, predicting a spreading and an extended form of the excitation, instead of localization. This makes it clear that regarding the focusing, we indeed encounter a nonlinear phenomenon.

Complementary information about the spreading or localization of the Gaussian excitation can be obtained from its time evolution in the reciprocal space, i.e.. in terms of the wave numbers $k \in [-\frac{\pi}{\Delta s}, \frac{\pi}{\Delta s}]$, where Δs denotes the arc length interparticle distance of the equidistant ground-state configuration. To this extent, we examine how the discrete

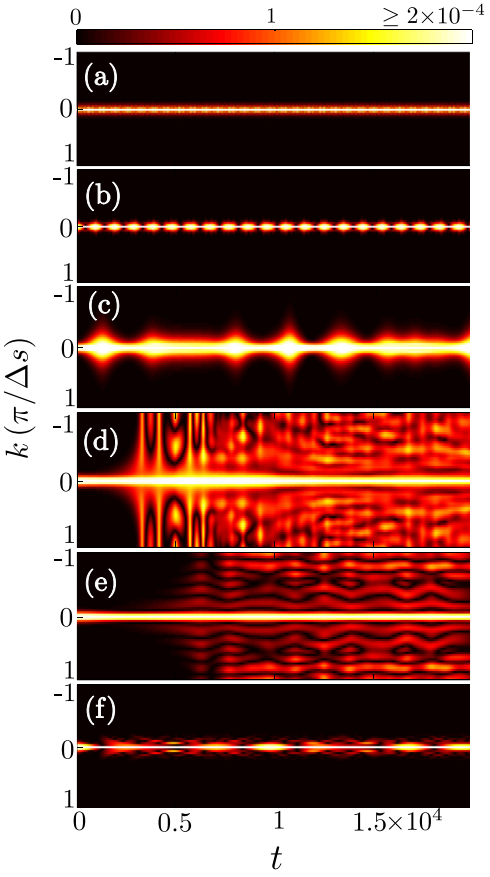

FIG. 3. (Color online) Absolute value of the discrete Fourier transform of the local energy excitation profile as a function of time and wave number k. (a)–(f) correspond to increasing r, ranging from r_0 to r_5 as indicated in Fig. 1(b).

Fourier transform of the local energy profile evolves in the reciprocal space [Figs. 3(a)–3(f)]. The initial excitation, being overall extended in the coordinate space [Fig. 1(c)], appears to be rather localized around the wave vector $k = 0$ in the k space. It remains localized as expected for $r < r_d$ [Figs. 3(a), 3(b)], but when approaching r_d more wave vectors in the vicinity of $k = 0$ become excited [Fig. 3(c)]. At the degenerate geometries [Figs. 3(d), 3(e)] the excitation expands rapidly in the reciprocal space, populating after the characteristic time t_F almost all the wave numbers k. The space localized solution consists therefore of most of the k modes, with the population of the initial $k = 0$ mode being dominant. At $r > r_d$ [Fig. 3(f)] the excitation remains, as for small r, in the narrow vicinity of the $k = 0$ mode.

Before proceeding with our study of the nonlinear behavior, let us note that for the results presented here we have used a rather small initial excitation with a total energy of the order of 1% of the ground-state energy per particle E_{GS}/N. For larger amplitudes the self-focusing can occur also for smaller radii, i.e., at a greater distance from the degeneracy region.

IV. EFFECTIVE NONLINEAR MODEL

The dynamics analyzed in the previous section is characterized by a self-focusing process of excitations for the case

of degenerate geometries and therefore suggests a prominent role of the nonlinearity. We aim in this section to identify and quantify the leading nonlinear terms as well as to derive a DNLS effective model in the region of degeneracy. As a result we will, among others, gain insight into the excitation amplitudes and the time scale t_F for localization.

A. Dominant nonlinear terms

Since the initial excitation is small enough we attempt to identify the dominant anharmonic terms by expanding the potential around the equilibrium configuration $\{u^{(0)}\}$ up to fourth order. It is advantageous to do so in the arc length parametrization s so that the final Euler-Lagrange equations of motion and particularly the kinetic terms would assume the standard form [26]. To this purpose we calculate the matrices

$$H_{ij} = \left.\frac{\partial^2 V}{\partial s_i \partial s_j}\right|_{\{s^{(0)}\}}, \quad G_{ij} = \left.\frac{\partial^3 V}{\partial s_i^2 \partial s_j}\right|_{\{s^{(0)}\}} \tag{4}$$

corresponding to the Hessian and the matrix of the third derivatives respectively. Terms involving more than two different positions are equal to zero, since the total potential V is a sum of exclusively two-body potential terms.

For the fourth derivative terms we define two further matrices as

$$M_{ij} = \left.\frac{\partial^4 V}{\partial s_i^2 \partial s_j^2}\right|_{\{s^{(0)}\}}, \quad Q_{ij} = \left.\frac{\partial^4 V}{\partial s_i^3 \partial s_j}\right|_{\{s^{(0)}\}} \tag{5}$$

for $i \neq j$ and

$$M_{ii} = Q_{ii} = \frac{1}{2}\left.\frac{\partial^4 V}{\partial s_i^4}\right|_{\{s^{(0)}\}},$$

separating the derivatives of the same order in s_i, s_j from those with a different order and splitting the diagonal derivative terms (involving differentiation with respect to a single position) in two. The calculation of the above derivatives in the arc length parametrization can be carried out by using the respective derivatives in the u coordinate space as well as the known relations for derivatives of inverse functions. Under these considerations and denoting $s_j - s_j^{(0)} = x_j$ the potential reads

$$\begin{aligned} V \approx E_{GS} &+ \frac{1}{2}\sum_{i,j=1}^{N} x_i H_{ij} x_j + \frac{1}{6}\sum_{i,j=1}^{N} x_i^2 G_{ij} x_j \\ &+ \frac{1}{24}\sum_{i,j=1}^{N} x_i^2 M_{ij} x_j^2 + \frac{1}{24}\sum_{i,j=1}^{N} x_i^3 Q_{ij} x_j \end{aligned} \tag{6}$$

leading to the equations of motion

$$\begin{aligned} \ddot{x}_n = &-\sum_{j\neq n} H_{nj} x_j - H_{nn} x_n - \frac{1}{3}\sum_{j\neq n} x_n G_{nj} x_j \\ &- \frac{1}{6}\sum_{j\neq n} G_{jn} x_j^2 - \frac{1}{6}\sum_{j\neq n} x_n M_{nj} x_j^2 - \frac{1}{3} M_{nn} x_n^3 \\ &- \frac{1}{8}\sum_{j\neq n} x_n^2 Q_{nj} x_j - \frac{1}{24}\sum_{j\neq n} Q_{jn} x_j^3, \end{aligned} \tag{7}$$

which consist of harmonic, quadratic, and third-order nonlinear terms. All the matrices appearing in these equations are symmetric except for the matrix G_{ij}, relating to the quadratic force terms, which is fully antisymmetric. This can affect significantly the symmetry of the expected solutions. If the quadratic nonlinear force terms are ignored then the equations of motion (7) possess the symmetry $x_n \to -x_n$ which also results in symmetric excitations keeping their symmetry in the course of propagation. The quadratic force terms, however, break the reflection symmetry and allow for an asymmetric evolution of initially symmetric excitations as the one observed in Fig. 2(d).

Let us mention at this point that in the ring limit $r = r_0 = 0$, where a separation of the center of mass holds, the matrices involved in Eq. (7) are not independent but obey the relations

$$H_{nn} = -\sum_{j\neq n} H_{nj}, M_{nn} = -\frac{1}{8}\sum_{j\neq n} Q_{nj}, M_{nj} = -\frac{3}{4} Q_{nj}$$

yielding

$$\begin{aligned} \ddot{x}_n = &-\sum_{j\neq n} H_{nj}(x_j - x_n) - \frac{1}{6}\sum_{j\neq n} G_{jn}(x_j - x_n)^2 \\ &- \frac{1}{24}\sum_{j\neq n} Q_{nj}(x_j - x_n)^3, \end{aligned} \tag{8}$$

which for only nearest-neighbor (NN) couplings leads to a Fermi-Pasta-Ulam kind of equations of motion [30], with both quadratic and cubic nonlinear interactions.

Before proceeding, we note that the matrix elements $H_{ij}, G_{ij}, M_{ij}, Q_{ij}$ depend, due to the symmetry of the ground-state configuration, only on the index difference $m = i - j$. Therefore, when referring to these elements in the following we will use the notation H_m, G_m, M_m, Q_m.

B. DNLS model

The effect of localization of the initial wave packet occurs, as we have observed in Sec. III, in the regime close to degeneracy. There, the diagonal terms of the Hessian provide the dominant contribution to the linear spectrum as the off-diagonal ones are very small. Since $|H_0| \gg 2|H_1|$ [Fig. 4(a)], one can use in that regime the so-called rotating wave approximation (RWA) [31], assuming that the position coordinate can be described as

$$x_n(t) = \Psi_n(t) e^{-i\omega_0 t} + \Psi_n^*(t) e^{i\omega_0 t}, \tag{9}$$

with $\Psi_n(t)$ a slowly varying amplitude and $\omega_0^2 = H_0$ yielding a fast oscillating phase $e^{\pm i\omega_0 t}$. Apart from the requirement of a weak dispersion, a condition for a sufficiently weak nonlinearity has also to be satisfied [31], namely $|H_0| \gg \frac{1}{3}|M_0| \max[x_i(0)]^2$ with $\max[x_i(0)]$ the maximum initial displacement (or respectively momentum) of a single particle. This criterion is satisfied as well in our case, since the initial conditions we have used lead to $|H_0|$ of about 100 times larger than $\frac{1}{3}|M_0| \max[x_i(0)]^2$.

Using the ansatz (9) and making the assumption $|\frac{d\Psi_n}{dt}| \ll \omega_0 |\Psi_n|$, as well as neglecting the rapidly oscillating terms with

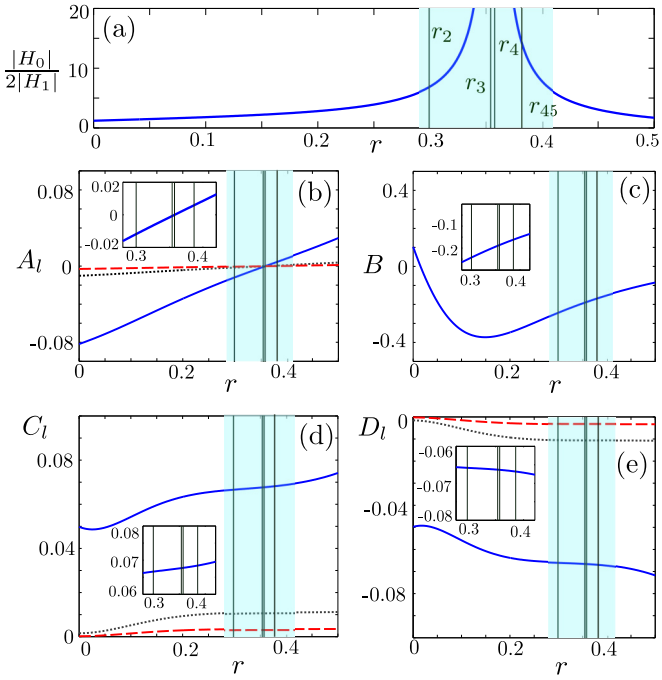

FIG. 4. (Color online) (a) The ratio between the diagonal and off diagonal elements of the Hessian $\frac{|H_0|}{2|H_1|}$ as a function of r. (b)–(e) Coefficients A_l, B, C_l, D_l defined in Eq. (11) as a function of r. The solid blue lines depict the coefficient values for $l = 1$, whereas the black doted lines for $l = 2$ and the red dashed ones for $l = 3$. The cyan (shaded) area marks the region of applicability of the RWA as derived from (a). The vertical lines correspond to the values of r we study with the DNLS model. Note that three of them namely r_2, r_3 and r_4 are the same as those studied in the previous section [Fig. 1(b)] whereas r_{45} lies between r_4 and r_5. The insets provide a zoom into the region of interest.

frequency $3\omega_0$, the equations of motion (7) acquire the form

$$
\begin{aligned}
i\dot{\Psi}_n = & \sum_{l=1}^{N/2} A_l(\Psi_{n-l} + \Psi_{n+l}) + B|\Psi_n|^2\Psi_n \\
& + \sum_{l=1}^{N/2} C_l\big[2\Psi_n(|\Psi_{n-l}|^2 + |\Psi_{n+l}|^2) + \Psi_n^*\big(\Psi_{n-l}^2 + \Psi_{n+l}^2\big)\big] \\
& + \sum_{l=1}^{N/2} D_l[2|\Psi_n|^2(\Psi_{n-l} + \Psi_{n+l}) + \Psi_n^2(\Psi_{n-l}^* + \Psi_{n+l}^*) \\
& + |\Psi_{n-l}|^2\Psi_{n-l} + |\Psi_{n+l}|^2\Psi_{n+l}] \\
& + \sum_{l=1}^{N/2} F_l\big[\big(2\Psi_n(\Psi_{n+l} - \Psi_{n-l}) - \Psi_{n+l}^2 + \Psi_{n-l}^2\big)e^{-i\omega_0 t} \\
& + (2\Psi_n(\Psi_{n+l}^* - \Psi_{n-l}^*) - |\Psi_{n+l}|^2 + |\Psi_{n-l}|^2)e^{i\omega_0 t}\big]
\end{aligned}
\tag{10}
$$

with

$$
A_l = \frac{H_l}{2\omega_0}, \quad B = \frac{M_0}{2\omega_0}, \quad C_l = \frac{M_l}{12\omega_0}
$$
$$
D_l = \frac{Q_l}{16\omega_0}, \quad F_l = \frac{G_l}{12\omega_0}. \tag{11}
$$

The last term in Eq. (10) comes from the quadratic nonlinear force term, which is responsible for generating second harmonics and breaking the reflection symmetry of the equations. Within the RWA this term is also neglected due to its fast oscillation in time in comparison to the other slowly varying terms. Of course such an approximation limits our consideration to the general focusing/defocusing behavior of the wave-packet excitation, not accounting for secondary propagation features such as the exact shape of the excitation pulse during the time evolution.

The actual numerical values of the remaining coefficients A_l, B, C_l, D_l for our system are shown in Figs. 4(b)–4(e) as a function of r. All the coefficients in the region of validity of our approximation have a definite sign except for A_l, which changes sign within the degeneracy regime. It is also obvious that an increasing index l leads to coefficients closer and closer to zero, with even the coefficients of $l = 2$ being already very small. Since the major contribution stems from $l = 1$, we can proceed performing a NN approximation, which yields

$$
\begin{aligned}
i\dot{\Psi}_n = & A(\Psi_{n-1} + \Psi_{n+1}) + B|\Psi_n|^2\Psi_n \\
& + C\big[2\Psi_n(|\Psi_{n-1}|^2 + |\Psi_{n+1}|^2) + \Psi_n^*\big(\Psi_{n-1}^2 + \Psi_{n+1}^2\big)\big] \\
& + D\big[2|\Psi_n|^2(\Psi_{n-1} + \Psi_{n+1}) + \Psi_n^2(\Psi_{n-1}^* + \Psi_{n+1}^*) \\
& + |\Psi_{n-1}|^2\Psi_{n-1} + |\Psi_{n+1}|^2\Psi_{n+1}\big],
\end{aligned}
\tag{12}
$$

where we have omitted the index 1 from the coefficients for clarity. Equation (12) can be recognized as a DNLS equation with additional nonlinear couplings studied in the literature [24,25] and will be the point of reference in the following discussion.

In order to check the validity of our approximation we propagate the Gaussian excitation illustrated in Fig. 1(c) according to Eq. (12). Note that the quantity Ψ is by definition complex, with its real part at $t = 0$ relating to the displacement $\mathrm{Re}(\Psi_n(0)) = \frac{x_n(0)}{2}$ [Eq. (9)] and its imaginary part to the momentum $\mathrm{Im}(\Psi_n(0)) = \frac{p_n(0)}{2\omega_0}$ [Eq. (9) within the RWA], both in the arc length parametrization. Furthermore, the local energy $E_n = \frac{1}{2}(\omega_0^2 x_n^2 + p_n^2)$ can be expressed as $E_n = 2\omega_0^2|\Psi_n|^2$, the conservation of the total energy being thus linked directly with the conservation of $\sum_n |\Psi_n|^2$. A comparison between Figs. 5(a)–5(c) and Figs. 2(c)–2(e) makes it clear that the NN DNLS model captures qualitatively very well the features of the exact excitation propagation, exhibiting focusing and defocusing at r_2 [Fig. 5(a)] and localization after a certain time for r within the degeneracy region [Figs. 5(b), 5(c)]. Beyond the point r_4, but still very close to the degeneracy [Fig. 4(a)], the excitation, although keeping its shape for a long time, eventually disperses into the whole crystal [Fig. 5(d)]. Note that the profile of the excitation remains reflection symmetric (with respect to the central particle) in the course of propagation for all geometries [Figs. 5(a)–5(d)], in contrast to what is observed in Fig. 2(d), which we attribute primarily to the neglected quadratic nonlinear term.

Most of these results can already be inferred from an inspection of Eq. (12) and the parameter $A(r)$ as shown in Fig. 4(b). When increasing the radius, A changes its sign from negative (same sign as B) to positive. Correspondingly, with increasing r the effective nonlinearity changes from attractive (hopping A and nonlinearity B of the same sign), leading to

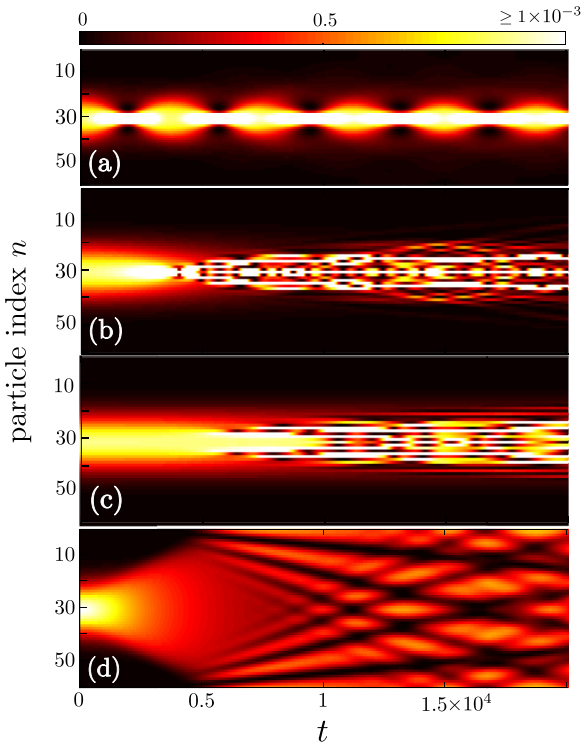

FIG. 5. (Color online) (a)–(d) Time propagation of the initial Gaussian excitation of Fig. 1(c) under the DNLS equation (12) for increasing r corresponding to the points (a) r_2, (b) r_3, (c) r_4, and (d) r_{45} marked in Fig. 4(a). Colors encode the values of local energy $E_n = 2\omega_0^2|\Psi_n|^2$ for each particle n and time t.

self-focusing dynamics [Figs. 5(a)–5(c)], to repulsive (hopping A and nonlinearity B of opposite sign), leading to defocusing [Fig. 5(d)].

The change of the magnitude of the parameter A affects also the degree and the time scale of the wave-packet localization. A small hopping term is expected to slow down the dynamical behavior of the system since it accounts for reduced mobility. A decrease in its magnitude leads also to an enhancement of the general nonlinear behavior since it shifts the weight of the dynamics to the nonlinear terms. On a more formal level, these statements can be justified within a multiple scale analysis [32].

In fact, one can arrive at the RWA by assuming that all the terms of Eq. (7) are much smaller than the $H_{nn}x_n$ term. Introducing the small parameter $\epsilon = |A|$, due to the weak coupling and weak nonlinearity conditions a slow time scale can be defined $\tilde{t} = \epsilon t = |A|t$, which is characteristic for the time evolution of Ψ_n. A further rescaling of Ψ_n with $\sqrt{|\frac{B}{A}|}$ leads to the standard form of our DNLS [24,25] with $\tilde{A} = \mathrm{sgn(A)}$, $\tilde{B} = \mathrm{sgn}(\frac{\mathrm{B}}{\mathrm{A}})$, $\tilde{C} = \frac{C}{B}$, $\tilde{D} = \frac{D}{B}$ and $\tilde{\Psi}_n = \sqrt{|\frac{B}{A}|}\Psi_n$ in which the strength of the nonlinearity is primarily controlled by the amplitude of the initial excitation $\tilde{\Psi}_n(0)$. In the degeneracy regime, due to the factor $\sqrt{|\frac{B}{A}|}$, this is about one order of magnitude larger than its value for other parameter values of r resulting in the observed strong localization of the excitation. In the same regime the time scale of the time evolution becomes very large, scaling as $\frac{1}{|A|}$ and yielding in our case a characteristic time t_F of the order of 10^3.

The simple picture above of the DNLS within the NN approximation gradually fails in the limit $|A| \to 0$, and the dispersion coefficients A_l from all the neighbors have to be incorporated into Eq. (12). This can be seen, for instance, from the intricate nonmonotonic features in the linear dispersion of the full model there [Fig. 1(b) (inset) below and close to r_4], which are not predicted by the NN DNLS model. Notably, however, even at r_4 our results within the NN DNLS model [Fig. 5(c)] capture satisfactorily the dynamics of the full system [Fig. 2(e)]. This can be attributed to the nonlinear coupling terms (C, D), which become stronger than the linear one (A) within this narrow parameter region and dominate the dispersion. As a last remark, we note that for long times the weak nonlinearity condition may also start to fail (if substantial amplitude has localized on a single site), such that the existence of higher harmonics becomes more prominent, which may lead to effects such as breaking of the parity symmetry.

V. BREATHERLIKE EXCITATIONS

Having constructed an effective DNLS model we can finally pose the question of the existence of breatherlike solutions in our system in the regime of degeneracy. If the coefficients C, D of Eq. (12) were zero, our system could be described within the so-called anticontinuum limit of weakly coupled oscillators, since the linear coupling is already very small. In this limit, it has been proven that discrete breather solutions exist if there is a substantial degree of anharmonicity and no resonances with the linear spectrum [33]. In our case with $C, D \neq 0$ one can still search for breathers provided, as well, that their frequency does not belong to the phonon spectrum [24]. To this end the frequency in the ansatz of Eq. (9) should be changed from ω_0 to $\omega < \omega_0$ out of the phonon band, i.e.,

$$x_n(t) = \Psi_n(t)e^{-i\omega t} + \Psi_n^*(t)e^{i\omega t}. \tag{13}$$

Repeating the steps of the previous section assuming that still the RWA holds, we arrive at Eq. (14) with an additional local term $\Lambda\Psi_n$

$$\begin{aligned} i\dot{\Psi}_n = {} & A'(\Psi_{n-1} + \Psi_{n+1}) + \Lambda\Psi_n + B'|\Psi_n|^2\Psi_n \\ & + C'\left[2\Psi_n(|\Psi_{n-1}|^2 + |\Psi_{n+1}|^2) + \Psi_n^*\left(\Psi_{n-1}^2 + \Psi_{n+1}^2\right)\right] \\ & + D'\left[2|\Psi_n|^2(\Psi_{n-1} + \Psi_{n+1}) + \Psi_n^2(\Psi_{n-1}^* + \Psi_{n+1}^*)\right. \\ & \left. + |\Psi_{n-1}|^2\Psi_{n-1} + |\Psi_{n+1}|^2\Psi_{n+1}\right], \end{aligned} \tag{14}$$

where $\Lambda = (\omega_0^2 - \omega^2)/2\omega$, $A' = A\frac{\omega_0}{\omega}$, $B' = B\frac{\omega_0}{\omega}$, $C' = C\frac{\omega_0}{\omega}$ and $D' = D\frac{\omega_0}{\omega}$. In the anticontinuum limit $A', C', D' = 0$ this equation can be easily checked to have the solutions $\Psi_n \in \{0, \sqrt{\frac{\Lambda}{B}}e^{i\phi_n}\}$ with arbitrary phases $\phi_n \in \mathbb{R}$. Simple real breather solutions can thus be constructed iteratively as strings of the elements 0 and $\pm\sqrt{\frac{\Lambda}{B}}$. Starting from such a breather solution and following the solution trajectories in the parameter space A', C', D' with a Newton method [24,34] we can find possible breather solutions for different values of r corresponding to the geometries of interest. The natural step then is to transform back to the x_n, p_n coordinates and use these as an initial

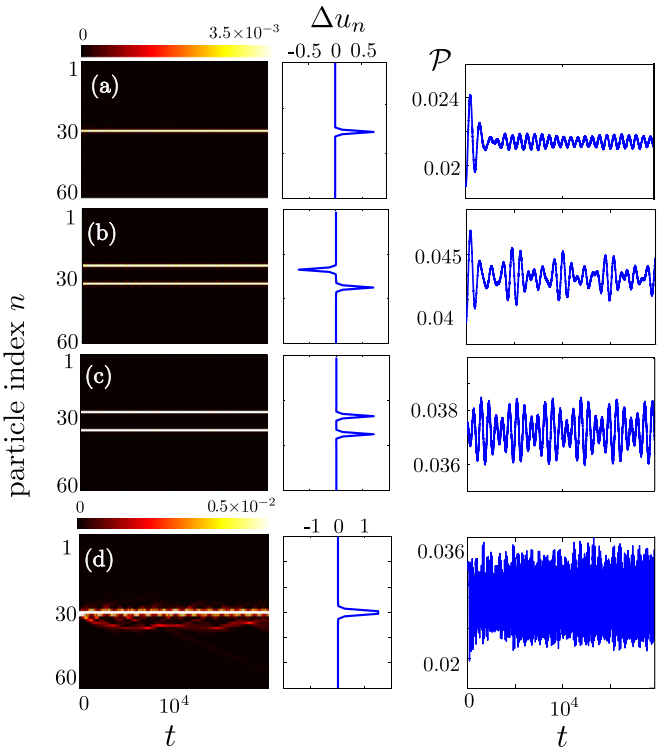

FIG. 6. (Color online) (a)–(d) Time propagation of breatherlike excitations in the degeneracy regime, at $r = r_3$ in (a), (b), (d), and $r = r_4$ in (c). The color plots of the first column depict the values of the local energy E_n whereas the second column provides the initial profiles of the excitation in position coordinates, i.e., $\Delta u_n = u_n - u_n^{(0)}$ as a function of the particle index n. The third column illustrates the time evolution of the participation ratio $\mathcal{P}$ for the degenerate geometries and the initial conditions of (a)–(d). In (a)–(d) the initial excitation comes only from the displacement Δu_n of particles from their equilibrium.

excitation in our system, simulating their time evolution within the full model equations as done in Sec. III. In this way, we aim to further substantiate the link between the effective DNLS equation and the full charges-on-a-helix model governed by the Lagrangian of Eq. (2), demonstrating that the prominent localized excitations of the DNLS also preserve their character in the full model.

Our results are presented in Fig. 6 for different initial conditions at the degenerate geometries. Evidently, many of them [Figs. 6(a)–6(c)] keep their solitonic character in the presence of the full Coulomb interactions, a fact that can be justified also by inspecting the time evolution of the participation ratio. Indeed, the local energy profile of the excitations changes negligibly with oscillating potential and kinetic energy parts, mapping to oscillating displacements Δu_n and momenta p_n. These breatherlike excitations include a single-particle excitation [Fig. 6(a)] as well as two-particle excitations with both opposite [Fig. 6(b)] and equal displacements [Fig. 6(c)].

Surprisingly enough, we have observed that the excited particles should always be separated by a distance [Figs. 6(b), 6(c)] for the solitonic character to persist, otherwise, if neighboring particles are excited there is always a small dispersion and a part of the excitation that focuses on a single particle, acquiring finally a rather asymmetric profile [Fig. 6(d)]. This picture is also valid within the DNLS framework where such solutions are found to undergo a spontaneous symmetry breaking in the course of propagation.

VI. SUMMARY AND CONCLUSIONS

We have shown that a system of charged particles confined on a toroidal helix can react in qualitatively different ways when exposed to an initial excitation, depending on the geometric properties of the confining manifold. In particular, while dispersion is the major feature of the dynamics for very small helix radii r, the excitation self-focuses and localizes for values of r in the so-called degeneracy regime, where the linear coupling is very small. Beyond this regime, the time evolution of the excitation is characterized by a defocusing, which is gradually dominated again by dispersion. Especially the self-focusing of the excitation observed for the degenerate geometries constitutes a hallmark of the existing nonlinearity in the system. Interestingly enough, the nonlinear part of the interactions (both local and nonlocal) does not approach zero in this regime, nor does it undergo a change in sign with increasing r, contrary to the behavior of the respective linear part. It is primarily this contrast between the robustness of the nonlinearity and the variability of the linear part, which induces the variety of dynamics in the system, allowing for its control through the tuning of the underlying geometry.

Furthermore, we have identified the character of the leading nonlinear terms and constructed an effective discrete nonlinear Schrödinger model with additional nonlinear couplings, which has allowed us to predict and interpret the different responses of the helical chain to its excitation. Through this model it has also been possible to identify some special breatherlike excitations in our system which propagate in time keeping their shape. Overall, we emphasize that the present setup offers many possibilities for the implementation of various nonlinear models ranging from the Fermi-Pasta-Ulam to different discrete nonlinear Schrödinger models with both attractive and repulsive nonlinearities only by the tuning of a single geometrical parameter, i.e., the radius r of the helix.

Regarding its possible experimental realization, it relies on the challenging task of constructing a helical trap for charged particles. Although such a construction might not be straightforward, there have been certain advances towards this direction in different contexts, such as the realization of freestanding helical nanostructures [35–37] and the design of helical traps for neutral atoms [38,39]. Moreover, our results could be of relevance in studies of energy and excitation transfer in helical molecules, such as DNA. Finally, macroscopic realizations of our system could also be possible by using for example charged beads as done for the study of polymers [40,41].

ACKNOWLEDGMENTS

A.Z. thanks the International Max Planck Research School for Ultrafast Imaging and Structural Dynamics for support in the form of a scholarship. J.S. gratefully acknowledges support from the Studienstiftung des deutschen Volkes.

APPENDIX: DEFINITION OF LOCAL ENERGIES

As briefly mentioned in Sec. III the definition of local energies E_n in a system of interacting particles is not unique. For a general potential $V = \frac{1}{2}\sum_{i,j,i\neq j}^{N} W(u_i,u_j)$ the most common partition consists in equally distributing each part of the potential energy among the particles involved

$$E_n = \frac{1}{2}\sum_{i,i\neq n}^{N} W(u_i,u_n) + K_n - E_n^{(0)}, \tag{A1}$$

with $E_n^{(0)} = \frac{1}{2}\sum_{i,i\neq n}^{N} W(u_i^{(0)},u_n^{(0)})$ the local energy of the equilibrium configuration $\{u_i^{(0)}\}$ and K_n the kinetic energy of the particle n. Although such a definition is very useful in describing systems with nearest-neighbor interactions such as oscillator chains [27,28], it can lead to problems concerning the description of long-range interacting systems and particularly those involving Coulomb interactions, as the one we consider in this paper. The major problem is that it generally leads to both positive and negative values of E_n and thus demands a handling of both positive and negative excitations. Negative local energies should be avoided if we wish to interpret the local energy as the amount or probability of the corresponding particle being excited and proceed in defining quantities such as the participation ratio $\mathcal{P}$ of Eq. (3).

Let us demonstrate this fact with a simple example of a Coulomb system consisting of three identical charges moving on a ring [Fig. 7(a)]. The equilibrium configuration of such as system is the equidistant one with the charges sitting in the corners of an equilateral triangle with a side of length y. Evidently then $E_n^{(0)} = \frac{1}{y}, n = 1,2,3$. If particle 1 is clockwise displaced from equilibrium up to the point $1'$ the resulting local excitation energies would be

$$E_1 = \frac{1}{2y_+} + \frac{1}{2y_-} - \frac{1}{y}, \quad E_2 = \frac{1}{2y_-} - \frac{1}{2y},$$
$$E_3 = \frac{1}{2y_+} - \frac{1}{2y},$$

where $y_+ > y > y_-$. Obviously $E_1, E_2 > 0$, whereas $E_3 < 0$, demonstrating that following this definition the local energy can become negative. Another minor disadvantage of this definition of local energy for long-range interacting particles is that it is highly nonlocal, meaning that if a single particle is displaced from equilibrium, the local energies of other particles even those far apart will acquire a finite value.

A way to fix this last issue is to construct the local energy E_n so that it contains: all the parts of the potential depending solely on u_n, none of the parts that are independent of u_n, and half of the terms involving both u_n and any other u_i. This can be written in a compact form

$$E_n = \frac{1}{2}\sum_{i,i\neq n}^{N}\left[W(u_n,u_i) + W\left(u_n,u_i^{(0)}\right)\right]$$
$$- \frac{1}{2}\sum_{i,i\neq n}^{N}\left[W\left(u_n^{(0)},u_i\right) + W\left(u_n^{(0)},u_i^{(0)}\right)\right] + K_n, \tag{A2}$$

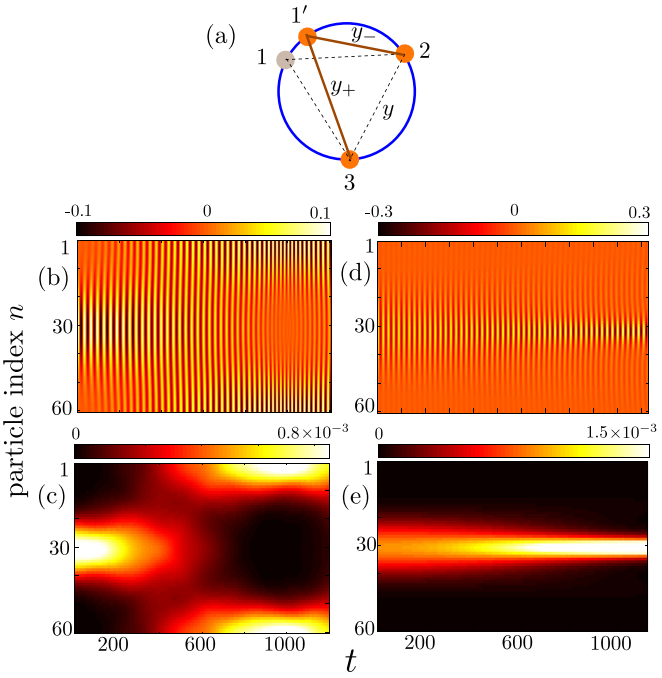

FIG. 7. (Color online) (a) A schematic illustration of three charges on a ring at equilibrium (1, 2, 3) and after particle 1 has been displaced (1′, 2, 3). The dashed lines denote the Euclidean distances in equilibrium, whereas the solid ones, the distances after the displacement. (b), (c) The time evolution of a Gaussian excitation for $r = r_1$. (d), (e) The time evolution of a Gaussian excitation for $r = r_2$. The colors in (b), (d) encode the values of the displacement from equilibrium x_n whereas in (c), (e) the values of the local energies E_n defined in Eq. (A5). (b)–(e) show simulation results for $N = 60$ particles and $\nu = 1/2$.

which can be checked to sum up to the total excitation energy, i.e., $\sum_{n=1}^{N} E_n = E$. Such a definition solves the problem of nonlocality since it distributes all single-particle potential terms to the corresponding particles, yielding for example $E_n = 0$ for $u_n = u_n^{(0)}$ and $K_n = 0$. It can also be checked to solve the problem of negativity in many cases, such as the one of the above three-particle example. There are however still special cases in which negative local energies can be encountered, where the negativity originates from the harmonic part of the total potential contained in each E_n

$$V_n^{(2)} = \frac{1}{2}\left.\frac{\partial^2 V}{\partial u_n^2}\right|_{(0)}\left(u_n - u_n^{(0)}\right)^2$$
$$+ \frac{1}{2}\sum_{i,i\neq n}^{N}\left.\frac{\partial^2 V}{\partial u_n \partial u_i}\right|_{(0)}\left(u_n - u_n^{(0)}\right)\left(u_i - u_i^{(0)}\right), \tag{A3}$$

which can assume negative values at a given n. To fix this, one can make use of the overall stability of the equilibrium, which leads to the existence of a different decomposition of the harmonic contributions to the potential into purely positive parts in the form [29]

$$\tilde{V}_n^{(2)} = \frac{1}{2}\left[\sum_{j=1}^{N}\Omega_{nj}\left(u_j - u_j^{(0)}\right)\right]^2, \tag{A4}$$

where Ω denotes the square root of the Hessian. We thus adjust our definition (A2) by subtracting $V_n^{(2)}$ and adding instead $\tilde{V}_n^{(2)}$, i.e.,

$$E_n = \frac{1}{2}\sum_{i,i\neq n}^{N}\left[W(u_n,u_i)+W\left(u_n,u_i^{(0)}\right)\right] - \frac{1}{2}\sum_{i,i\neq n}^{N}\left[W\left(u_n^{(0)},u_i\right)+W\left(u_n^{(0)},u_i^{(0)}\right)\right] + K_n - V_n^{(2)} + \tilde{V}_n^{(2)}. \quad \text{(A5)}$$

This definition provides a sufficiently local (although not entirely, due to the term $\tilde{V}_n^{(2)}$), positive decomposition of the excitation energy, which still satisfies $\sum_{n=1}^{N} E_n = E$. Its use can be further justified by comparing the time evolution of E_n with the time evolution of the displacement of the particle n from equilibrium $x_n = s_n - s_n^{(0)}$. A comparison of Figs. 7(b), 7(d) with 7(c), 7(e) respectively, leads to the conclusion that the time evolution of E_n captures nicely all the features of the propagating excitation such as the focusing and the spreading and only filters out the fast oscillations in Figs. 7(b), 7(d) caused by the fast continuous conversion of potential to kinetic energy and vice versa.

[1] A. C. Scott, *Nonlinear Science* (Oxford University Press, Oxford, 1999).
[2] S. A. Akhmanov, A. P. Aukhorukov, and R. V. Khokhlov, Sov. Phys. Usp. **10**, 609 (1968).
[3] J. C. Eilbeck, P. S. Lomdahl, and A. C. Scott, Physica D **16**, 318 (1985).
[4] M. Johansson, M. Hörnquist, and R. Riklund, Phys. Rev. B **52**, 231 (1995).
[5] A. J. Sievers and S. Takeno, Phys. Rev. Lett. **61**, 970 (1988).
[6] M. Remoissenet, *Waves Called Solitons: Concepts and Experiments* (Springer-Verlag, Berlin, 1999).
[7] D. K. Campbell, S. Flach, and Yu S. Kivshar, Phys. Today **57**, 43 (2004).
[8] P. G. Kevrekidis, *The Discrete Nonlinear Schrödinger Equation* (Springer-Verlag, Heidelberg, 2009).
[9] D. N. Christodoulides and R. I. Joseph, Opt. Lett. **13**, 794 (1988).
[10] R. Morandotti, U. Peschel, J. S. Aitchison, H. S. Eisenberg, and Y. Silberberg, Phys. Rev. Lett. **83**, 4756 (1999).
[11] A. A. Sukhorukov, Yu S. Kivshar, H. S. Eisenberg, and Y. Silberberg, IEEE J. Quantum Electro. **39**, 31 (2003).
[12] A. Trombettoni and A. Smerzi, Phys. Rev. Lett. **86**, 2353 (2001).
[13] F. Kh. Abdullaev, B. B. Baizakov, S. A. Darmanyan, V. V. Konotop, and M. Salerno, Phys. Rev. A **64**, 043606 (2001).
[14] H. Hennig, J. Dorignac, and D. K. Campbell, Phys. Rev. A **82**, 053604 (2010).
[15] S. F. Mingaleev *et al.*, J. Biol. Phys. **25**, 41 (1999).
[16] M. Peyrard, Nonlinearity **17**, R1 (2004).
[17] A. Dang Koko *et al.*, Chaos **22**, 043110 (2012).
[18] Yu B. Gaididei, S. F. Mingaleev, and P. L. Christiansen, Phys. Rev. E **62**, 53(R) (2000).
[19] J. F. R. Archilla, P. L. Christiansen, and Yu B. Gaididei, Phys. Rev. E **65**, 016609 (2001).
[20] B. Sánchez-Rey, J. F. R. Archilla, F. Palmero, and F. R. Romero, Phys. Rev. E **66**, 017601 (2002).
[21] P. G. Kevrekidis, S. V. Dmitriev, S. Takeno, A. R. Bishop, and E. C. Aifantis, Phys. Rev. E **70**, 066627 (2004).
[22] S. Takeno, S. V. Dmitriev, P. G. Kevrekidis, and A. R. Bishop, Phys. Rev. B **71**, 014304 (2005).
[23] A. V. Zampetaki, J. Stockhofe, and P. Schmelcher, Phys. Rev. A **91**, 023409 (2015).
[24] M. Öster, M. Johansson and A. Eriksson, Phys. Rev. E **67**, 056606 (2003).
[25] M. Öster and M. Johansson, Phys. Rev. E **71**, 025601(R) (2005).
[26] A. V. Zampetaki, J. Stockhofe, S. Krönke, and P. Schmelcher, Phys. Rev. E **88**, 043202 (2013).
[27] A. Sarmiento, R. Reigada, A. H. Romero, and K. Lindenberg, Phys. Rev E **60**, 5317 (1999).
[28] D. Hennig, S. Fugmann, L. Schimansky-Geier, and P. Hänggi, Phys. Rev E **76**, 041110 (2007).
[29] P. B. Allen and J. Kelner, Am. J. Phys. **66**, 497 (1998).
[30] E. Fermi, J. Pasta, and S. Ulam, Los Alamos, Report No. LA-1940 (1955); G. P. Berman and F. M. Izrailev, Chaos **15**, 015104 (2005).
[31] Yu. S. Kivshar and M. Peyrard, Phys. Rev. A **46**, 3198 (1992).
[32] C. M. Bender and S. A. Orszag, *Advanced Mathematical Methods for Scientists and Engineers* (McGraw-Hill, New York, 1978).
[33] R. S. MacKay and S. Aubry, Nonlinearity **7**, 1623 (1994).
[34] J. L. Marín and S. Aubry, Nonlinearity **9**, 1501 (1996).
[35] V. Y. Prinz *et al.*, Physica E **6**, 828 (2000).
[36] O. G. Schmidt and K. Eberl, Nature (London) **410**, 168 (2001).
[37] *Nanotubes and Nanofibers* edited by Y. Gogotsi (Taylor & Francis, New York, 2006).
[38] E. Vetsch, D. Reitz, G. Sagué, R. Schmidt, S. T. Dawkins, and A. Rauschenbeutel, Phys. Rev. Lett. **104**, 203603 (2010).
[39] D. Reitz and A. Rauschenbeutel, Opt. Comm. **285**, 4705 (2012).
[40] M. Reches, P. W. Snyder, and G. M. Whitesides, Proc. Nat. Acad. Sci. USA **106**, 17644 (2009).
[41] S. Tricard *et al.*, Phys. Chem. Chem. Phys. **14**, 9041 (2012).